Science of the Total Environment 771 (2021) 144810

Contents lists available at ScienceDirect

Science of the Total Environment

journal homepage: www.elsevier.com/locate/scitotenv

Impacts of the evolving urban development on intra-urban surface thermal environment: Evidence from 323 Chinese cities

Huimin Liu [a], Bo Huang [a,b,*], Sihang Gao [c], Jiong Wang [d], Chen Yang [e], Rongrong Li [a]

[a] Institute of Space and Earth Information Science, The Chinese University of Hong Kong, Shatin, NT, China
[b] Department of Geography and Resource Management, The Chinese University of Hong Kong, Shatin, NT, China
[c] School of Urban Design, Wuhan University, Wuhan 430072, China
[d] Faculty of Geo-Information Science and Earth Observation, University of Twente, Enschede 7500, the Netherlands
[e] College of Urban and Environmental Sciences, Peking University, Beijing 100871, China

HIGHLIGHTS

- 82% of the cities were cooler in the generally larger-sized new urban areas expanded since 1992.
- Elevation difference, NDVI difference, and Gini coefficient present spatially varying relationships with LST difference.
- Elevation difference dominates explaining the LST difference for most cities.

GRAPHICAL ABSTRACT

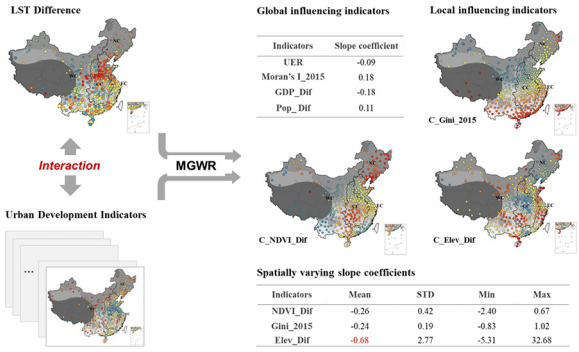

ARTICLE INFO

Article history:
Received 26 September 2020
Received in revised form 23 December 2020
Accepted 23 December 2020
Available online 26 January 2021

Editor: Ashantha Goonetilleke

Keywords:
LST
Urban development
Intra-urban
Old and new urban areas
MGWR
China

ABSTRACT

Urban development has significantly modified the surface thermal environment in urban areas. This study provides the first attempt to characterize the urban development imprint on surface thermal environment for 323 cities across the entire country of China, using an intra-urban perspective. Specifically, it investigates the variation of surface thermal environment in terms of land surface temperature (LST) difference triggered by significant urban evolution of intra-urban division containing two primary classes: old urban areas developed by 1992 and new ones expanded in the 1992–2015 period. Under this "old-new" dichotomy, the relationship between urban development and the LST difference is explored through Multi-scale Geographically Weighted Regression (MGWR). Results reveal that urban development is closely related to the difference in LST between old and new urban areas in 2015, which varies from −2.66 °C to 2.46 °C, up to −6.27 °C in western China. 264 cities manifest relatively "cooler" urban environments in the generally larger-sized new urban areas. The seven selected urban development indicators can explain 75% of the variance in the LST difference through MGWR. Among them, the old-new elevation difference, the normalized difference vegetation index (NDVI) difference, and Gini coefficient are found to influence the LST difference in various spatially varying manners. The elevation difference, a generally underestimated nature-driven indicator, is found dominant in explaining the LST difference for 252 cities, among which 216 cities demonstrate higher LSTs in the urban areas with lower elevations. Overall, this study provides valuable information of human-environment interaction across many cities in a generalized way, which complements similar studies at local level, and helps to depict a complete picture of

* Corresponding author at: Institute of Space and Earth Information Science, The Chinese University of Hong Kong, Shatin, NT, China.
E-mail addresses: hmliu@cuhk.edu.hk (H. Liu), bohuang@cuhk.edu.hk (B. Huang), SihangGao@whu.edu.cn (S. Gao), j.wang-4@utwente.nl (J. Wang), cyangcues@stu.pku.edu.cn (C. Yang), rongrongli@cuhk.edu.hk (R. Li).

https://doi.org/10.1016/j.scitotenv.2020.144810

environmental impacts of urban development. The integrated workflow can also be promoted to other periods or other countries to examine the corresponding urbanization imprint on intra-urban surface warming.

1. Introduction

Urban areas, which are home to more than half of the world's population (Seto et al., 2017), are experiencing additional warming compared to the global mean due to the direct impact of urbanization on local thermal environment (Foley et al., 2005; Stone, 2012; Estrada et al., 2017). This urbanization-induced local warming exposes urban dwellers to extra heat stress (Li et al., 2020). Its impact on human health is further exacerbated given its non-linear interactions with regional and global climate change (Patz et al., 2005; Manoli et al., 2019). In addition to health risks, it also poses negative effects on energy consumption, air and water quality and urban ecosystems (Foley et al., 2005; Grimm et al., 2008).

Existing literature regarding the urbanization-induced local warming has been mainly following an "urban-rural" dichotomy, where urban areas are treated as a whole against its non-urban surroundings. The research object of such a dichotomy, the Urban Heat Island (UHI) effect, depicts a phenomenon of urban areas exhibiting elevated temperature compared to their rural surroundings (Grimm et al., 2008; Oke et al., 2017). The UHI effect has been extensively assessed across the globe and testified the "urban-rural" dichotomy as effective in measuring how much the urban climate has been modified relative to its background conditions under urbanization (Oke et al., 2017; Li et al., 2019; Manoli et al., 2019). Nevertheless, the dichotomy considers urban areas holistically and thus inevitably ignores the heterogeneous temperature patterns within urban areas. In fact, the intra-urban temperature patterns are intrinsically spatially varying due to the diversified urban forms and urban functions (Stewart and Oke, 2009; Liu et al., 2019a) shaped by complicated socio-economic, political and natural factors. On account of such spatially varying patterns, the heat stress posing to urban dwellers is also not evenly distributed. To facilitate better understanding of intra-urban temperature patterns and the urbanization-temperature relationship, a break away from the "urban-rural" dichotomy is necessary. Therefore, we may utilize the various intra-urban patterns within a city as natural laboratories to identify both problems and solutions to local warming mitigation and adaptation (Jia and Zhao, 2020).

Furthermore, current UHI-based studies are generally local-dominated, although ensemble or cross-sectional comparison across large spatial domains is essential in achieving understandings of common features or fundamental differences (Oke, 1973; Zhou et al., 2017). According to a recent review summarizing relevant studies using satellite remotely sensed Land surface temperature (LST) data during the 1972–2018 period, local studies dominate 64%, while evidently less attention (14%) has been paid to cross-city comparison at large scales (Zhou et al., 2019). Moreover, the majority of the existing large-scale studies tend to cover only large cities, especially in China (Zhou et al., 2014; Wang et al., 2015; Zhou et al., 2014, 2016; Yao et al., 2017) where unprecedented urbanization has been in fact witnessed for all-sized cities. These large-city dominated studies leaves the worldwide small cities under-represented, although they hold 43% of the world urban population (Lamb et al., 2019) and are projected to accommodate even larger proportion in the future (Chai and Seto, 2019). Given the urban developments in large and small cities can be different (Chai and Seto, 2019; Lamb et al., 2019; Güneralp et al., 2020), the urban heat problems and the corresponding driving factors in smaller cities are not necessarily equivalent to those of large cities and yet to be explored. Hence, a large-scale study with sufficient all-sized city samples, which provides a consistent analytical environment and thus enables generality and difference recognition of urban heat problems, may shed new light on our understanding of the urbanization-induced local warming.

Considering the above two limitations of existing UHI-based studies, an intra-urban perspective aiming at large scales may provide new insights into the urbanization imprint on urban thermal environment. In fact, intra-urban studies under the field of urban microclimate are well-documented, with the targeted urban units vary from facets (10×10 m) to local climate zones (2×2 km) (Oke et al., 2017). These studies characterize the unique form of local thermal environment with a high level of detail and generate knowledge which is crucial in developing localized policies (Martilli et al., 2020). In addition to these localized efforts, cross-sectional studies targeting on a large number of cities are also essential in achieving generalized knowledge for climatic modelling, urban planning and temperature projection. The challenge is, to find a universal intra-urban classification scheme suiting cross-sectional investigation at large scales. A contrast perspective of old and new urbanized areas divided based on the urban expanding process may serve for such understanding. The dynamic process of urban expansion modifies the spatial structure, socio-economic and ecological functions of urban systems (Lemoine-Rodríguez et al., 2020), which may collectively lead to the thermal difference between urban areas expanded in different periods. Overall, the advantage of such an old-new contrast perspective is twofold. First, it provides an opportunity to examine if the urbanization imprint on the thermal environment varies along with the process of urban expansion. It is noteworthy that, the selection of the years to define old and new urban areas is flexible, hence, any two years witnessing significant urbanization phase shifts or policy interventions can be used to explore the corresponding intra-urban thermal variations and possible differentiation of policy footprints. Second, it is advantageous in cross-sectional investigation compared to the conventional UHI paradigm. It measures intra-urban variation that involves no rural reference, thus largely weakening the interference from the diversified cooling effects and types of rural land covers which are largely manipulated by background climates.

Given the geographical and climatic diversities across large spatial domains, it is essential to take spatial non-stationarity into consideration while exploring how urban development impacts the old-new thermal variation. Spatial non-stationarity, a common nature of geographical processes depicting spatially varying relationships (Goodchild, 2004; Anselin, 2010; Murakami et al., 2018), has been extensively detected in the urbanization-temperature relationship based on the pixel level on a city-by-city basis (Su et al., 2012; Sun et al., 2018; Liu et al., 2019b). Nevertheless, it has been largely neglected when the relationship is analyzed across large spatial domains (Peng et al., 2011; Clinton and Gong, 2013; Zhou et al., 2014; Tan and Li, 2015; Yao et al., 2017; Zhou et al., 2017). Exceptionally, Li et al. (2017) captured the spatially varying response of surface UHI (SUHI) to the increase of urban area size across the conterminous United States and explicitly applied the geographically weighted regression (GWR) to measure the spatial heterogeneity. Numerous studies have also revealed the cooling effect of urban vegetation to be spatially varying across different climatic conditions (Spronken-Smith and Oke, 1998; Mills et al., 2010; Manoli et al., 2019; Yu et al., 2020). In fact, the propensity for anisotropic

dependence structures and non-stationarity tends to increase as the scope of the study expands (Finley, 2011), thus making spatial non-stationarity non-negligible in large-scale investigations. To capture spatial non-stationarity, the Multi-scale Geographically Weighted Regression (MGWR), a state-of-the-art geospatial technique, can be a more effective approach compared to the classic GWR (Fotheringham et al., 2017; Liu et al., 2019b; Yang et al., 2019a). Specifically, MGWR is able to allow the processes to operate not only locally as enabled by GWR, but also at various spatial scales (Fotheringham et al., 2017). Based on the spatially varying modelling results, it provides an opportunity to better understand the nature of geographic processes. Besides, we may identify the most influential indicators on the temperature difference, and provide geographically targeted references to mitigate local surface warming and minimize intra-urban thermal variation.

To fill the gaps above, the present study aims at large scale across the entire country of China, and investigates the urban development imprint on intra-urban surface thermal environment for 323 cities. In response to this aim, it specifically addresses the following aspects: (1) assess the intra-urban variation of surface thermal environment in terms of land surface temperature (LST) difference between old and new urban areas expanded in specific periods; (2) model the relationship between urban development and the LST difference using MGWR so that the possible spatial non-stationarity and scale-dependence of the responsive processes can be captured. This study will provide a new lens on the urbanization-induced local surface warming with three unique contributions: (1) large region coverage with numerous city samples, (2) intra-urban comparative perspective, (3) spatial non-stationary and scale-dependent relationships. The remainder of this paper describes the material and methods (Section 2), results (Section 3), discussion (Section 4), and conclusions (Section 5).

2. Material and methods

2.1. Study area

In this study, 323 cities distributed across the entire country of China are selected to assess the LST difference between old and new urban areas in 2015, based on the existence of old urban areas built by 1992, the occurrence of urban expansion during the 1992–2015 period, and also data availability. The 323 cities cover four administrative levels. From top to the bottom, they cover 4 centrally administrated municipalities (CAMs) of China, 15 sub-provincial cities, 17 provincial capital cities, and 287 prefecture-level cities. The cities also across all eight climate zones in China (Liu et al., 2020) (Fig. 1a). Overall, the selected 323 cities occupy 99.63% of the total urban areas, 98.30% of the population and 99.15% of the economic growth in China in 2015 (NBSC, 2016). Hence, the study area is adequate to provide a comprehensive sample size to study the relationship between urban development and urban surface thermal environment in China. Specifically, a start year of 1992 is selected according to the timing of significant policy intervention, urbanization phase shift in China, and land cover data availability. On one hand, in the 1990s (the third urbanization phase in China) and thereafter, all-sized cities across the entire country experienced rapid urban expansion with extensive constructions of new cities, high-tech parks and industrial development parks (Ye et al., 2006; Wu et al., 2014). Such an urbanization phase shift may be largely a result of the first urban planning law in China implemented in 1990, requiring the highly promotion of small cities, properly development of medium-sized cities, and expanding control of large cities (Wei, 1994). On the other hand, the land cover data used in this study, the competitive and extensively used (Song et al., 2019; Martilli et al., 2020; Liu et al., 2020) Land Cover (LC) products provided by the Climate Change Initiative of the European Space Agency (ESA-CCI LC), are only available since 1992. Therefore, to seek a compromise, we finally choose 1992 as the starting year to analyze the corresponding urban development patterns and the consequent surface thermal variations. During the 1992–2015 period, radical urban development has been witnessed in the country, as shown in Fi g. 1b in terms of both urbanization rate and economic growth.

2.2. Datasets

Multi-source data is used in this study. First, Moderate Resolution Imaging Spectroradiometer (MODIS) LST product is used to represent the urban surface thermal environment. Specifically, the MODLT1M, a monthly mean MODIS/Terra LST product (acquired at 10:30, 1-km-resolution) provided by the Geospatial Data Cloud of Computer

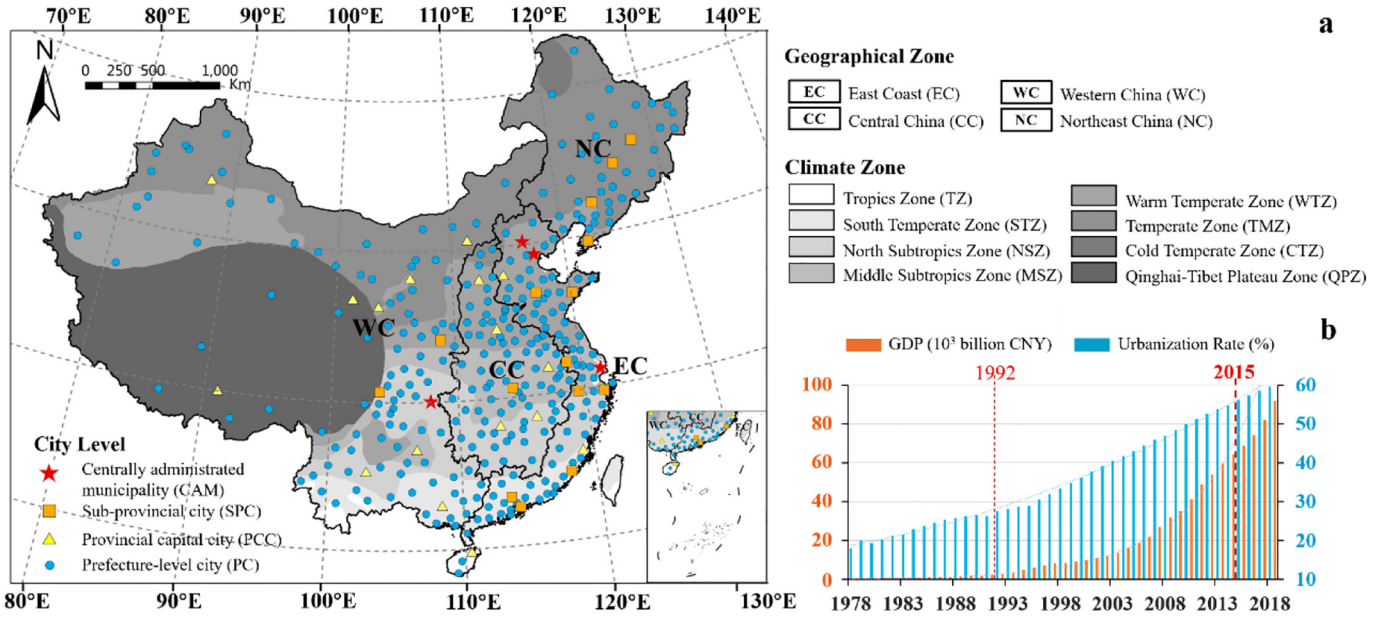

Fig. 1. (a) Distributions of the 323 cities; (b) The Gross Domestic Product (GDP) growth and urbanization rate in China from 1978 to 2018 (NBSC, 1979-2019) (the main study year of 2015 and the auxiliary year of 1992 used to divide old and new urban areas are highlighted).

Network Information Centre of Chinese Academy of Sciences (GSD) (2015), is used to generate the annual mean LST for 2015. The MODLT1M product itself is generated based on the daily LST product of MOD11A1, which is calculated through the generalized split-window LST algorithm and claimed to be with an accuracy higher than 1 °C (0.5 °C in most cases) (Wan, 2008). In fact, the good accuracy, together with its superior spatial and temporal resolutions, has already enabled MODIS LST products to be the second most popular LST data sources (25%) as summarized in a recent review (Zhou et al., 2019). The proportion can be much higher for large-scale studies. Second, ESA-CCI LC products (ESA, 2015) are used to identify the urban areas in China respectively in 1992 and 2015. The "urban" class in the LC maps was derived using two state-of-the-art global urban footprint databases (ESA, 2018): the Global Human Settlement Layer (Pesaresi et al., 2016) and the Global Urban Footprint (Esch et al., 2017). The overall weighted-area accuracy of the LC maps reaches around 71.7% according to the user guide. Third, for the indicators representing the multiple facets of urban development, MODIS MODND1M products (500-m-resolution) provided by GSD (2015) are resampled to 1 km and then used to generate the annual normalized difference vegetation index (NDVI) data for 2015. Besides, 1 km Grid datasets of Digital Elevation Model (DEM), GDP and population are also downloaded from the data center for Resources and Environmental Sciences, Chinese Academy of Sciences (RESDC) (2015) to represent the topographical and socio-economic conditions of the cities in 2015. A summary of all links of data sources used in this study is provided in Table S1 in the Supplementary material.

2.3. Methodology

2.3.1. The LST difference between old and new urban areas

In this study, an old-new contrast perspective is employed to depict the intra-urban surface thermal variation based on the urban expanding process. Specifically, to measure urban development from a landscape urbanization perspective and further identify urban areas for this study, the urban development intensity (UDI) (Imhoff et al., 2010; Zhou et al., 2016) is adopted. UDI is defined as the proportion of the 300 m × 300 m "urban" class in the ESA-CCI LC data in each 1 km × 1 km pixel (the resolution of the MODIS LST data) (Zhou et al., 2016). The areas with an UDI over 50% (Imhoff et al., 2010; Zhou et al., 2016; Liu et al., 2020) are identified as the urban areas on the 1-km scale for 1992 and 2015. Further, old urban areas (OUAs) are defined as urban areas developed by 1992 while new urban areas (NUAs) refer to the newly expanded urban areas thereafter up until 2015 (Song et al., 2019). Considering the certain de-urbanization phenomenon in China during the study period (Fu et al., 2019), OUAs are thus a subset of urban areas in 2015 and 1992 (Yao et al., 2017). Based on the differentiation of OUAs and NUAs, the LST difference in 2015 is than calculated, as shown in formula 1. It is noteworthy that, by using LST data of only 2015, other than the LST of OUAs in 1992 and that of NUAs in 2015, we can avoid the LST variation between 1992 and 2015 induced by the change of solar thermal radiation, inter-annual climate patterns, and also regional to global climate change (Liu et al., 2019a). Therefore, the impact of urban development on the LST difference can be exclusively analyzed. Besides, the impact of urban renewal on the LST patterns in old urban areas can also be covered in the analysis.

$$LST_D = LST_{OUA} - LST_{NUA} \quad (1)$$

where LST_D denotes the LST difference between OUAs and NUAs, LST_{OUA} represents the averaged LST value in OUAs, LST_{NUA} is the averaged LST value in NUAs.

The expanding characteristics of the urban areas and the old-new LST difference will be further analyzed using multiple division systems to investigate the corresponding statistical patterns. Specifically, this study employs three division systems respectively based on administrative levels, geographical and economic conditions, and background climate conditions, as shown in Fig. 1a.

2.3.2. Urban development indicators

An initial set of nine urban development indicators are selected for multicollinearity and significance tests, according to the efficacy of illustrating intra-urban LST variation and computational efficiency for large city samples. Old and new urban areas, developed under differentiated urban dynamics and policy guidance, may differ in urban area size, landscape composition, landscape configuration, socio-economic levels, and even topography, which collectively give rise to divergent thermal responses in these two types of areas. Hence, in this study, first, indicators regarding urban extent, including the log 10 of the final urban area size in 2015 and the urban expansion rate (UER) from 1992 to 2015, are selected given the significant magnifying effect of urban area size on UHI as revealed in previous studies (Zhou et al., 2013, 2017; Tan and Li, 2015; Li et al., 2017). Second, this study considers the widely-recognized warming effect of built-up areas (Zhou et al., 2014, 2016; Yang et al., 2019a) and cooling effect of vegetation (Zhou et al., 2014; Liu et al., 2018; Peng et al., 2018). Hence, two landscape composition indicators, the old-new differences of UDI and NDVI, are also covered. Third, the global Moran's I (Fan and Myint, 2014; Wang et al., 2019b) and the Gini coefficient (Liu et al., 2020), are employed to characterize the inequality level of landscape urbanization for their computational efficiency over large regions compared to conventional landscape configuration indicators. The primary difference between these two indicators lies in the ability of Moran's I to take spatial information into inequality assessment (Wei, 2015). Fourth, elevation (Zhou et al., 2014), a topographical feature of the urban areas, is also taken into account given the temperature drop trend with the rising of elevation (Peng et al., 2020) and also its significant restriction on urban expansion (Dubovyk et al., 2011; Li et al., 2018). Last, socio-economy development, as a key component of urban development and also sources of anthropogenic heat release (Huang and Cadenasso, 2016; Peng et al., 2018; Chen et al., 2020; Wang et al., 2020), is also considered. The description of the nine selected indicators is presented in Table 1. Multicollinearity and significance tests will run among the indicators and those passing the multicollinearity threshold measured by the variance inflation factor (VIF) less than 7.5 (Li et al.,

Table 1
Comprehensive information about the selected indicators.

Categories of indicators	Indicators	Descriptions
Urban extent	Urban size_2015	The log 10 of the urban areas size in 2015 (Li et al., 2017).
	UER	The proportion of NUAs in the total urban area in 1992 (Long et al., 2018).
Landscape composition	UDI_Dif	The difference of the averaged UDI between OUAs and NUAs in 2015.
	NDVI_Dif	The difference of the averaged NDVI between OUAs and NUAs in 2015.
Landscape configuration	Moran's I_2015	The global Moran's Is (Anselin et al., 2006) depicting the levels of spatial agglomeration of the urban areas for each city in 2015. It is calculated based on UDI, where those pixels with UDI < 0.5 (rural areas) are excluded.
	Gini_2015	The Gini coefficients (Bendel et al., 1989) depicting the levels of UDI inequality within each city in 2015.
Topography	Elev_Dif	The difference of the averaged elevation between OUAs and NUAs in 2015.
Socio-economy	GDP_Dif	The difference of the averaged GDP/km^2 between OUAs and NUAs in 2015.
	Pop_ Dif	The difference of the averaged Population/km^2 between OUAs and NUAs in 2015.

2010) with statistical significance ($p < 0.05$), will be reserved for further modelling.

2.3.3. Regression modelling and evaluation

The relationships between LST difference and the selected indicators are investigated through MGWR using an open-source platform (https://sgsup.asu.edu/sparc/mgwr). Hence, the spatial non-stationarity and scale-dependence of the responsive processes can be effectively captured. The contribution of each indicator to the LST difference is measured using the corresponding slope coefficients generated by the model. In addition to MGWR, the ordinary least squares (OLS) and the classic Geographically Weighted Regression (GWR) are also applied benchmarking the performance of MGWR. Theoretically, OLS ignores geospatial variations of the relationship between LST difference and the selected indicators, while GWR brings the variation into consideration, and MGWR further advances the consideration by taking the scale of the variation into account (Fotheringham et al., 2017). The formulas for OLS and GWR are listed in the Supplementary material, here we depict how MGWR models the relationship (Fotheringham et al., 2017):

$$LST_{Di} = \beta_0(u_i, v_i) + \sum_k \beta_{bwk}(u_i, v_i) X_{ik} + \varepsilon_i \quad (2)$$

where (u_i, v_i) represents the spatial coordinates of location i, X_{ik} denotes the kth indicator at location i, $\beta_0(u_i, v_i)$ is the intercept value, $\beta_{bwk}(u_i, v_i)$ denotes the kth slope coefficient at observation i under the optimal bandwidth of bwk, and finally ε_i is the Gaussian error at location i. Specifically, $\beta_{bwk}(u_i, v_i)$ is estimated through the following formula:

$$\widehat{\beta_{bwk}}(u_i, v_i) = \left[X^T W(u_i, v_i) X\right]^{-1} X^T W(u_i, v_i) Y \quad (3)$$

where $W(u_i, v_i)$ represents the weighting matrix allocating the observations close to the specific location a larger weight in the estimation. In this study, the fixed Gaussian kernel (Li et al., 2010; Zhao et al., 2018) is used:

$$w_{ij} = \exp\left(-\frac{d_{ij}^2}{b^2}\right) \quad (4)$$

where d_{ij} represents the Euclidean distance between location i and j, b denotes the fixed bandwidth. Specifically, the weighting value will be set as 1 if location j coincides with a i, and the w_{ij} for the surrounding locations will decrease gradually according to a Gaussian curve as the distance d_{ij} increases (Fotheringham et al., 2002).

The performances among MGWR, GWR and OLS will be evaluated using the coefficient of determination (R^2), the corrected Akaike information criterion (AICc) and the residual sum of squares (RSS) (Zhao et al., 2018; Liu et al., 2019b). A higher R^2, together with lower values of AICc and RSS, indicates a higher fitting degree of the model. The

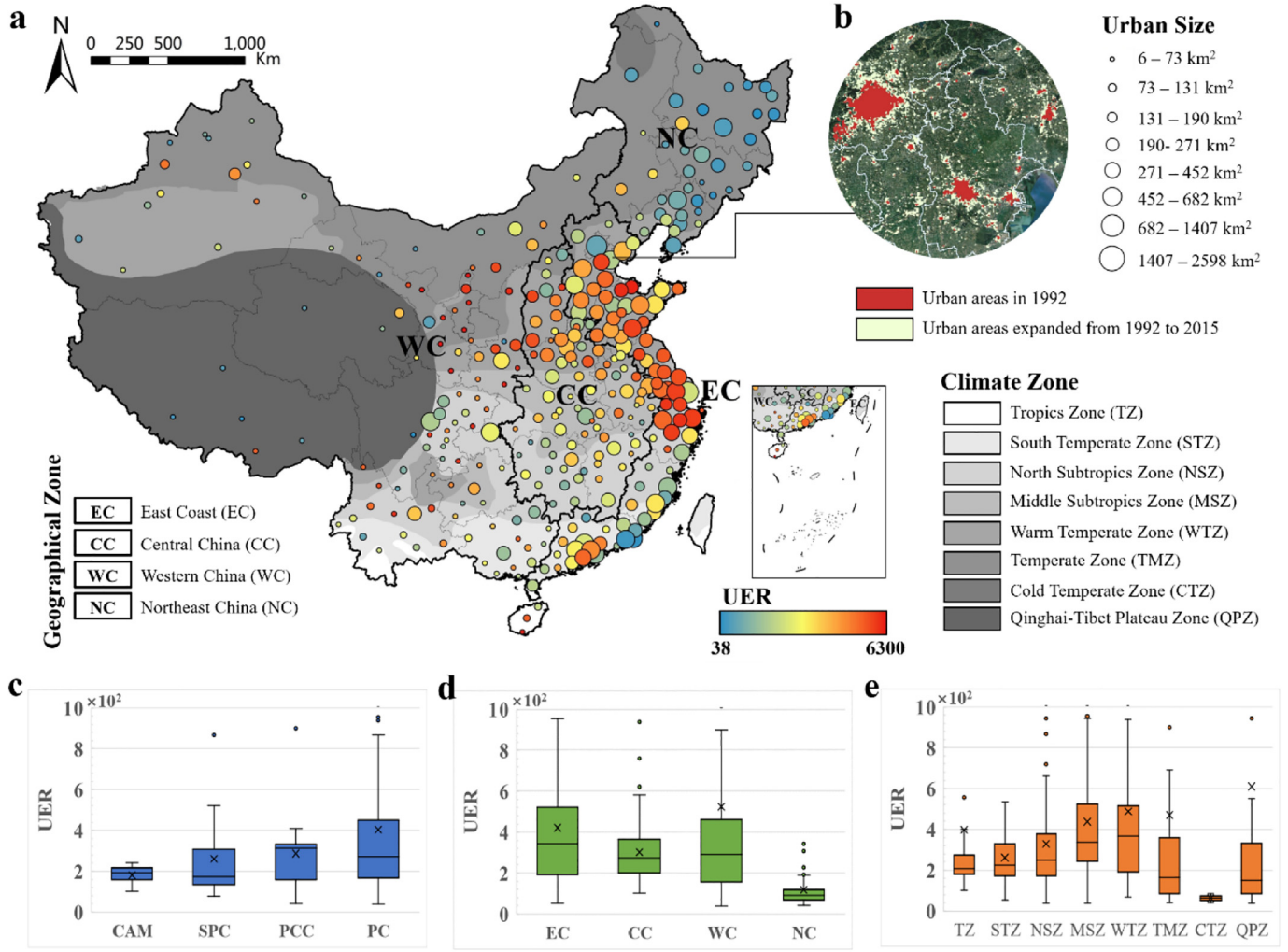

Fig. 2. Urban expansion among the 323 cities in China: (a) spatial distribution of UER and the urban area size in 2015; (b) the urban expanding process from 1992 to 2015 by taking the Beijing-Tianjin-Hebei region as example; boxplots of the UER (c) at four administrative levels; (d) in the four geographical zones; (e) in the eight climate zones.

formulas used to calculate the AICc and RSS are listed in the Supplementary Material.

3. Results

3.1. Urban expansion

Urban expansion, the basis for identifying old and new urban areas in this study, is firstly analyzed to generate a basic understanding of urban development in terms of landscape urbanization. Remarkable urban expansion is observed with significant spatial unevenness (Fig. 2a). The UER for the 323 cities ranges from 38% to 6300% with an average of 388%, indicating a larger size of new urban areas for the vast majority of cities. Generally, cities with higher administrative levels manifest smaller averaged magnitudes of urban expansion (Fig. 2c). Geographically, small-sized cities in the mid-west and large cities along the north east coast exhibit the largest expansion magnitudes, while northeast China experienced evidently less urban expansion (Fig. 2a, d). In regard to the eight climate zones in China (Fig. 2e), it is interesting to observe that many cities with high UER are located in moderate temperature zones such as the warm temperature zone and middle subtropics zone.

3.2. The LST difference between old and new urban areas

The LST difference between OUAs and NUAs is observed with significant regional discrepancy (Fig. 3). It covers a wide range from −2.66 °C to 2.46 °C except for the extreme value of −6.27 °C for Nyingchi in the Tibet Autonomous Region, and the mean value reaches 0.51 °C. Most cities (82%) exhibit higher LSTs in OUAs. Generally, larger positive LST differences are mainly observed in the North China Plain, while larger negative values tend to occur more sparsely in western and central China. The boxplot (Fig. 3b) further reveals that, contrary to the patterns of UER (Fig. 2c), generally cities with higher administrative levels demonstrate larger averaged LST differences, except for prefecture-level cities. It is interesting to notice that the LST differences for sub-provincial cities are more concentrated in distribution than those for provincial capital cities (Fig. 3b), although the two types of cities share equivalent sample sizes. Great spatial unevenness is also observed based on the four geographical zones (Fig. 3c). Among them, northeast China which expanded the least (Fig. 2d) manifests the largest averaged LST difference (0.74 °C). In regard to the eight climate zones, cities in the warm temperature zone demonstrate the highest averaged LST difference (0.72 °C) and also the largest value range (Fig. 3d). Combined with the findings in Section 3.1, many cities located in the warm temperature zone are either growing radically with higher UERs (Fig. 2e) or also producing larger LST differences (Fig. 3d).

3.3. The spatial patterns of the selected indicators

Seven indicators are finally selected after the multicollinearity (VIF < 7.5, actually all<5.0) and significance ($p < 0.05$) tests, including UER, NDVI_Dif, Moran's I_2015, Gini_2015, Elev_Dif, GDP_Dif and POP_Dif. Among them, UER has been preliminarily analyzed in

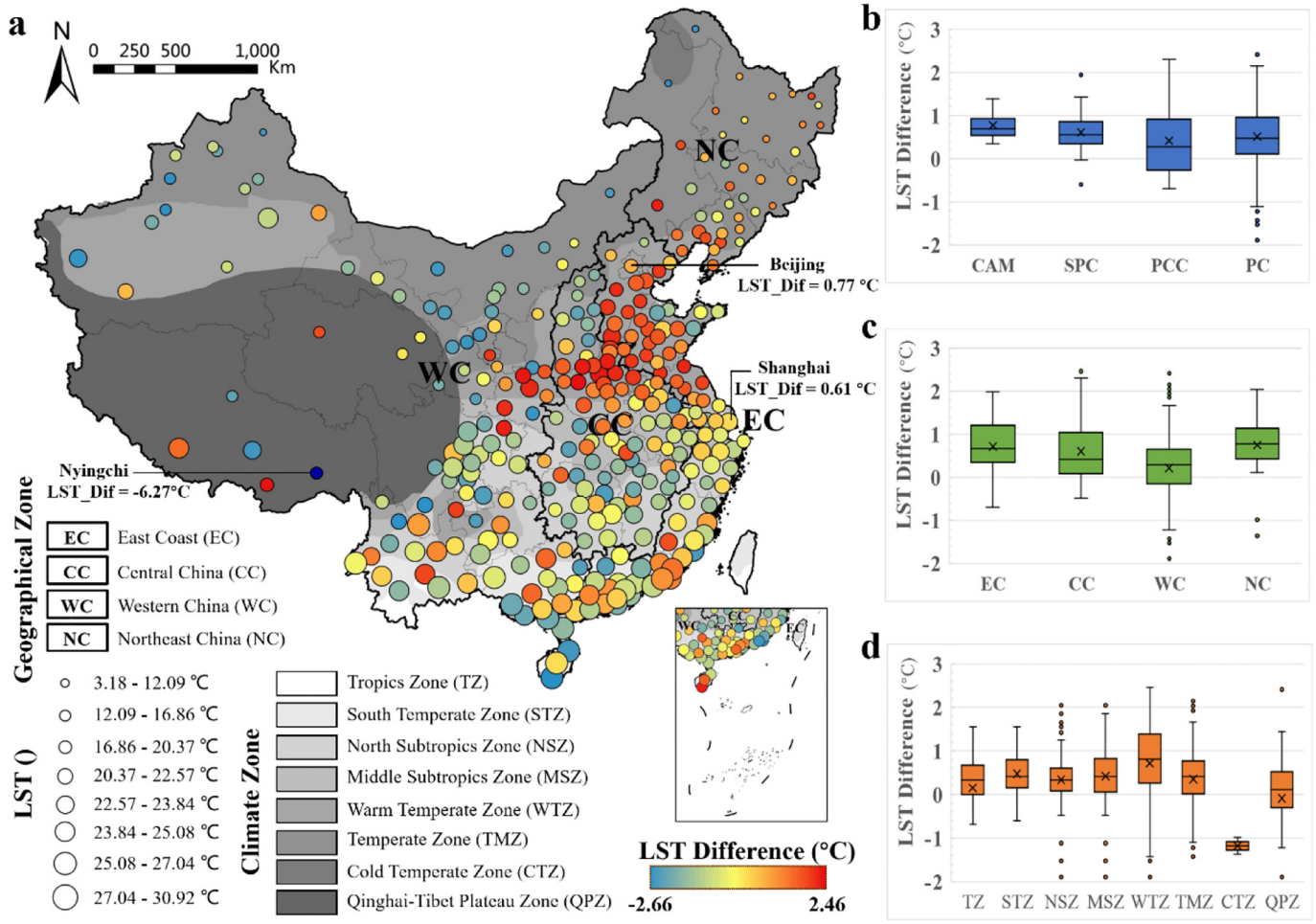

Fig. 3. (a) The LST difference among the 323 cities in China; boxplots of the LST difference (b) at four administrative levels; (c) in the four geographical zones; (d) in the eight climate zones.

Section 3.1 given its importance on the identification of old and new urban areas. Here, we present the distribution patterns of the remaining six indicators (Fig. 4). The averaged NDVI for NUAs is larger than that of OUAs for most cities (92%) (Fig. 4a). Among them, larger negative NDVI difference, similar to the larger positive LST difference in Fig. 2, tends to mainly occur in cities located in the warm temperature zone. In contrast, larger positive NDVI difference primarily distributes in western China. As for the global Moran's I, 94% of the cities demonstrate positive values, meaning significant spatial agglomeration patterns of the urban areas. The majority of the cities with greater agglomeration patterns are located in the warm temperature zone (Fig. 4b), to a large extent resembling to the clustering pattern of larger positive LST differences (Fig. 2). The spatial pattern of the Gini coefficient is somewhat opposite with that of the global Moran's I on the national scale, although they are also similar for a few cities, such as those located in the southeast coast. Generally, the more to the west, the greater regional inequality of landscape urbanization as witnessed with higher values of the Gini coefficient. In terms of elevation, most cities (59%) reveal higher values in NUAs than OUAs. Larger difference, whether positive or negative, are observed in western China which is dominantly mountainous areas with complicated topographical conditions. Specifically in the Tibet Autonomous Region, Nyingchi (2.179 km) and Shannan (1.861 km) demonstrate extreme values of elevation difference above 1 km. These two cities developed part of their new urban lands in the southern area with evident low altitudes, thus resulting in the extremely larger elevation differences. In regard to socio-economic conditions, most cities exhibit higher levels in OUAs in terms of both GDP (90%) and population (90%) per square kilometer. These two indicators share similar patterns on the national scale, while discrepancies also exist locally for a few cities. Generally, negative values are mainly observed in western China, signifying better socio-economic development in newly expanded urban areas in this under-developed mountainous region.

3.4. Performance of MGWR

MGWR is superior to OLS and GWR in terms of goodness-of-fit in modelling the relationship between LST difference and the selected urban development indicators, as evaluated by the three indices (Table S2 in the Supplementary material). All indices improve evidently from OLS to GWR and ultimately reach the optimal regression fit of MGWR. For instance, the R^2 of MGWR reaches a high level of 0.75, which is slightly higher than that of MGWR (0.70) and way surpasses that of OLS (0.35). This means that spatial heterogeneity is a non-negligible factor for capturing the relationship between urban development and intra-urban surface thermal environment. Besides, it is important to encode multi-scale information in modelling urbanization-temperature relationship.

As shown in terms of optimal bandwidths optimized by MGWR in Table 2, the relationships between LST difference and the selected indicators are modeled at different spatial scales. It is clearly that, compared to GWR which allocates a consistent scale (382.55 km) to all processes, MGWR successfully identifies the individual scales specific to each process. Specifically, the relationships between LST difference and NDVI_Dif, Gini_2015, and Elev_Dif exhibits spatial non-stationarity at various local scales (optimal bandwidths of 207.51 km, 412.88 km, and 158.47 km, respectively). On the contrary, UER, Moran's I_2015, GDP_Dif and Pop_ Dif tend to correlate with the LST difference in consistent global manners across China.

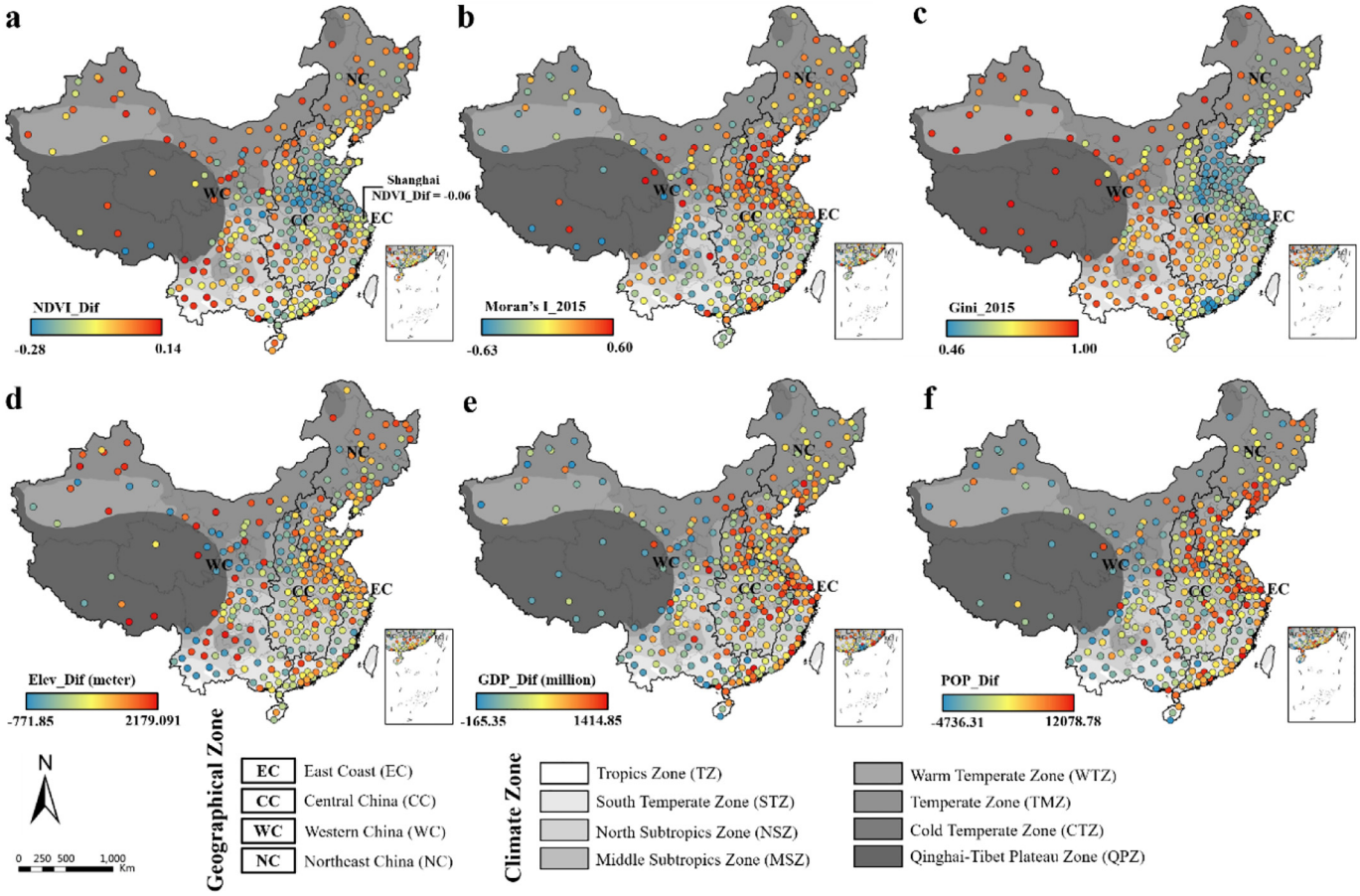

Fig. 4. The spatial distributions of the six indicators. (a) NDVI_Dif, (b) Moran's I_2015, (c) Gini_2015, (d) Elev_Dif, (e) GDP_Dif, (f) POP_Dif.

Table 2
Optimal bandwidths and slope coefficients of the selected indicators identified by MGWR.

Indicators	Optimal bandwidths	Slope coefficients			
		Mean	STD	Min	Max
UER	9077.10	−0.09	0.00	−0.09	−0.09
NDVI_Dif	207.51	−0.26	0.42	−2.40	0.67
Moran's I_2015	9077.33	0.18	0.00	0.18	0.18
Gini_2015	412.88	−0.24	0.19	−0.83	1.02
Elev_Dif	158.47	−0.68	2.77	−5.31	32.68
GDP_Dif	9073.59	−0.18	0.00	−0.18	−0.18
Pop_ Dif	9077.33	0.11	0.00	0.11	0.11

Note: bandwidth larger than 4539 km, the maximum distance between any two cities, is identified as global scale.

3.5. The relationships between LST difference and the urban development indicators

The relationships between LST difference and the seven indicators are further explored through the slope coefficients generated by MGWR (Table 2). Generally, although the relationships with NDVI_Dif, Gini_2015, and Elev_Dif demonstrate spatially varying patterns across China, we can still conclude that, for most cities, Elev_Dif exhibits the most significant correlation with a mean coefficient of −0.68, followed by NDVI_Dif (−0.26) and Gini_2015 (−0.24). Specifically, Elev_Dif dominates explaining the LST difference for 252 cities (78%), among which 216 cities demonstrate negative relationships between LST difference and Elev_Dif. Moran's I_2015 and GDP_Dif tend to influence the LST difference in a consistent degree of 0.18 although in the opposite ways. In comparison, the relationships with Pop_ Dif (0.11) and UER (−0.09) are the weakest.

The spatially varying slope coefficients of NDVI_Dif, Gini_2015, and Elev_Dif are further analyzed (Fig. 5). NDVI_Dif is negatively correlated with the LST difference in 262 cities (81%). That is, the urban areas with more abundant vegetation manifest a relatively lower average LST. Nevertheless, for the other 61 cities, which are mainly located in the temperature zone, north and middle subtropics zones, the NDVI_Dif manifests a positive relationship on the LST difference. Again, a boxplot analysis provides aggregated pattern at the climate zone level (Fig. 5d). The averaged slope coefficients demonstrate an overall inverted U-shape, indicating larger negative impacts from NDVI_Dif tend to occur in regions with higher or cooler temperature levels. In regard to Gini_2015, larger Gini produces smaller LST difference for the majority of the cities, except for the 6 cities located in the Qinghai-Tibet Plateau Zone, which are normally with sparsely distributed urban areas. Boxplot analysis (Fig. 5e) further reveals that, except for the Qinghai-Tibet Plateau Zone, regions with cooler background demonstrate greater negative impacts of Gini_2015. In terms of Elev_Dif, its decrease is related with an elevated LST difference for 263 cities (81%). That is, the urban areas with higher elevations exhibit a relatively lower average LST. Nevertheless, the relationship is contrast for the remaining 60 cities located as in clusters across China (Fig. 5f).

We further detail the relationships modeled by MGWR for 21 urban agglomerations in China (Fig. 6a). The urban agglomerations, identified on the prefecture city-level referring to public documents and previous studies (Long et al., 2018), account for 65% of the total urban areas, 70% of national GDP and 49% of the population in China in 2015. They are ranked from 1 to 21 by their final urban area sizes in 2015. All urban agglomerations expanded rapidly during the study period (Fig. 6b). Among them, 18 urban agglomerations exhibit higher averaged LSTs in OUAs, with 14-Central Plains (1.72 °C), 20-Beijing-Tianjin-Hebei (1.21 °C), and 10-Guanzhong Plain (1.14 °C) leading the LST differences (Fig. 6c). The averaged slope coefficients generated by MGWR further reveal Elev_Dif to be the dominant factor driving the LST differences for these three urban agglomerations, followed by the averaged Gini_2015 and NDVI_Dif (Fig. 6d, e, Table 2). In contrast, 3 urban

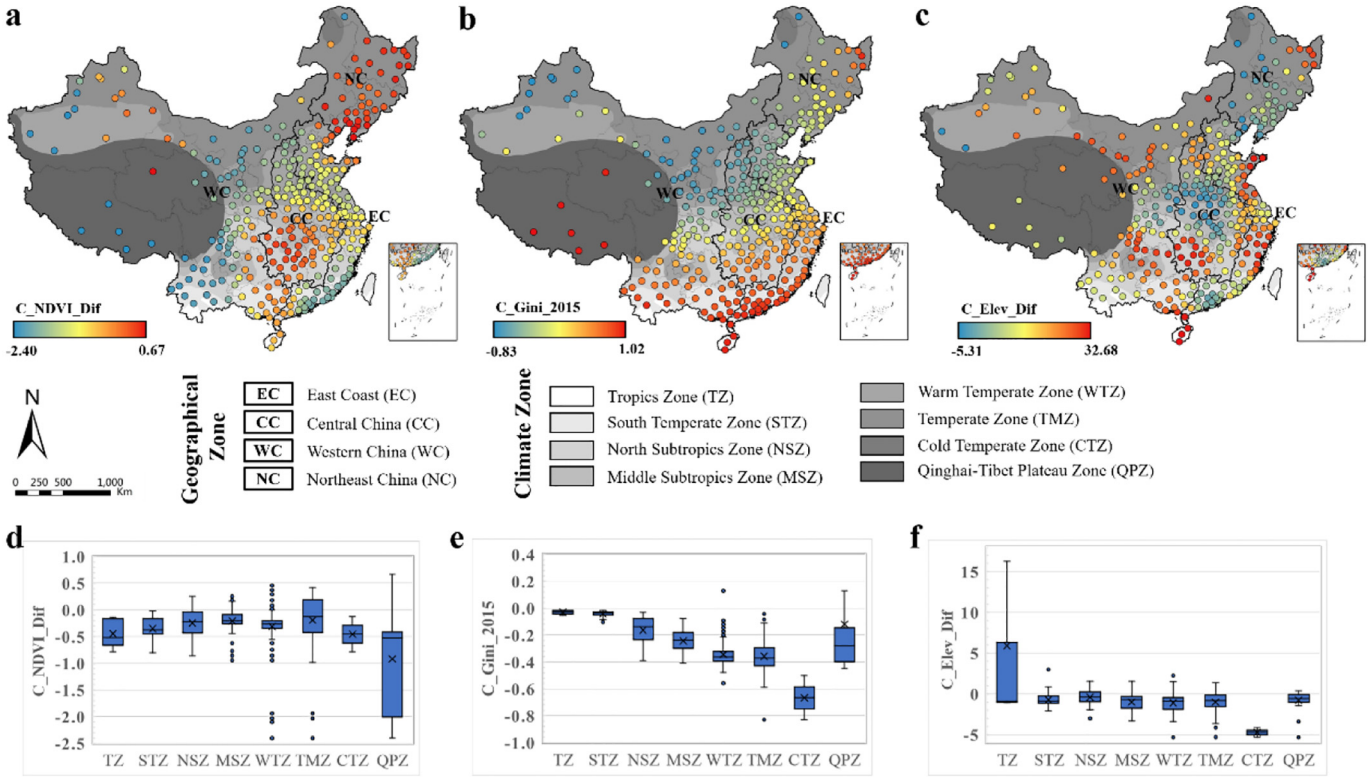

Fig. 5. The spatially varying slope coefficients of the indicators: (a) NDVI_Dif, (b) Gini_2015, and (c) Elev_Dif; and the corresponding boxplots based on the eight climate zones: (d) NDVI_Dif, (e) Gini_2015, and (f) Elev_Dif.

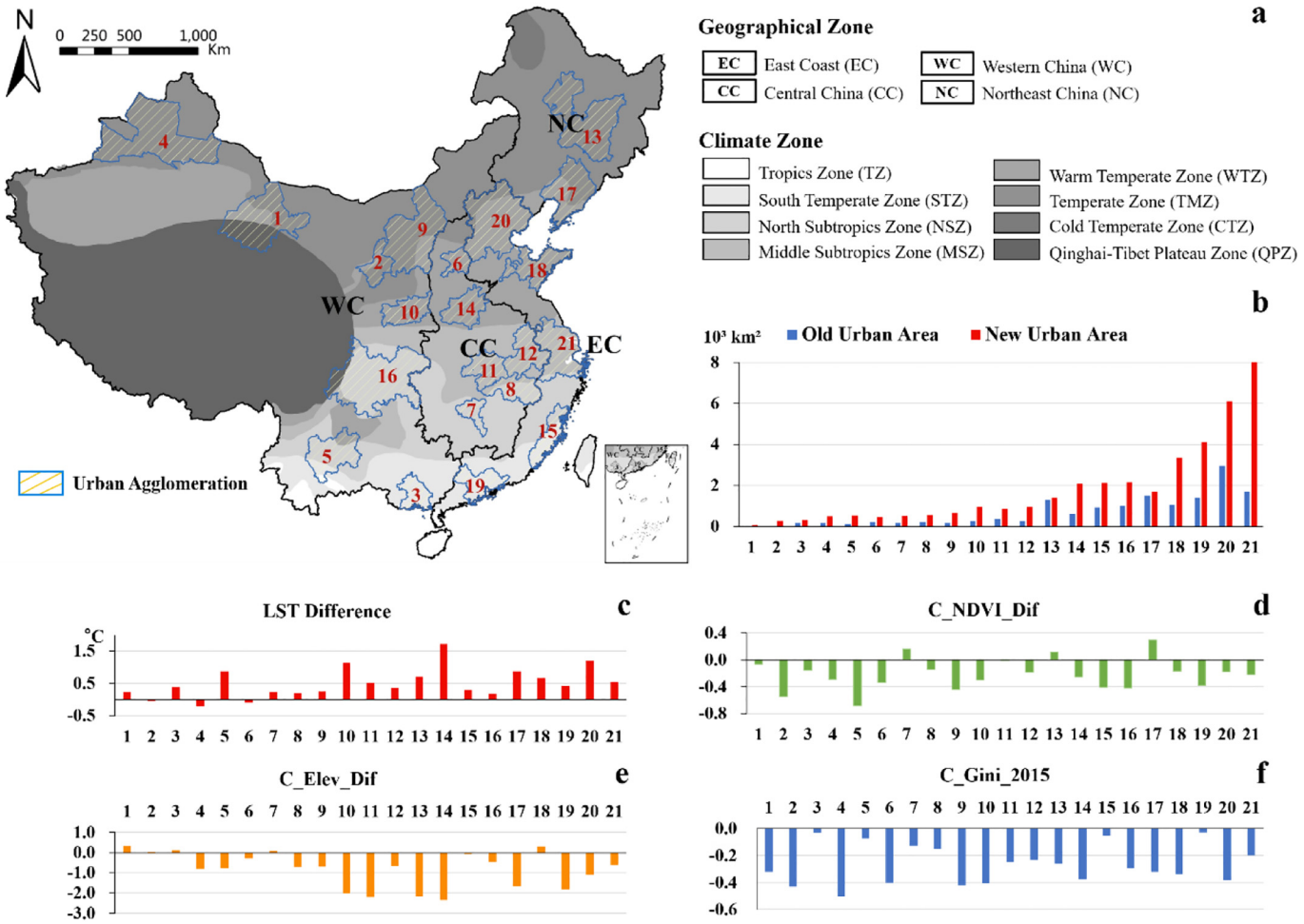

Fig. 6. (a) The 21 urban agglomerations in China; the bar graphs for the averaged (b) urban area sizes of old and new urban areas and (c) LST difference; the bar graphs for the averaged slope coefficients of (d) NDVI_Dif, (e) Elev_Dif and (f) Gini_2015. The x axis following the sequence of 1–21 depicts the serial numbers of the 21 urban agglomerations. Note: 1. Jiuquan-Jiayuguan-Yumen, 2. Northern Ningxia, 3. Beibu Gulf, 4. Northern Tianshan Mountain, 5. Central Yunnan, 6. Central Shanxi, 7. Changsha-Zhuzhou-Xiangtan, 8. Northern Jiangxi, 9. Hohhot-Baotou-Ordos-Yulin, 10. Guanzhong Plain, 11. Greater Wuhan, 12. Central Anhui, 13. Harbin-Changchun, 14. Central Plains, 15. Eastern Fujian, 16. Chengdu-Chongqing, 17. Liaodong Peninsula, 18. Shandong Peninsula, 19. Guangdong-Hong Kong-Macao Greater Bay, 20. Beijing-Tianjin-Hebei, 21. Yangtze River Delta.

agglomerations, including 4-Northern Tianshan Mountain, 6-Central Shanxi, and 2-Northern Ningxia, manifest higher LSTs in NUAs. Among them, 4-Northern Tianshan Mountain exhibits the largest positive elevation difference (93.29 m) among the 21 urban agglomerations (Table S3 in the Supplementary material). The larger elevation in OUAs may have greatly contributed to its lowered LST.

4. Discussion

This study investigates the intra-urban LST variation at large scale using a comparative perspective of old and new urban areas, and analyzes the impacts from urban development through MGWR. It covers 323 Chinese cities with diversified urban sizes, economic levels and climatic contexts. Hence, in contrast to the previous SUHI-based studies concerning only big cities (Zhou et al., 2016; Yao et al., 2017), the under-presented small- and medium-sized cities in China, which are developing rapidly but with lagging governance capacity (Lamb et al., 2019; Güneralp et al., 2020), can also benefit from the generalized knowledge and city-specific characteristics investigated in this study.

4.1. Patterns of the old-new LST difference

Uneven difference in LST between old and new urban areas is observed across the 323 Chinese cities. Most of them (82%) were with lower LSTs in the newly developed urban areas in 2015, which partly deciphers why declining trends of surface UHII (SUHII) were observed in part of Chinese cities, even under global warming (Zhou et al., 2016; Liu et al., 2020). The LST difference varies significantly across the 323 cities (Fig. 3) and 21 urban agglomerations (Fig. 6). Combined with the divisional statistical analysis, the regional discrepancy is collectively affected by cities' administrative levels (Fig. 3b), geographic and economic conditions (Fig. 3c), and also macroscopic climatic backgrounds (Fig. 3d). For example, the 15 sub-provincial cities manifest a more concentrated distribution of LST difference in contrast to the 17 provincial capital cities (Fig. 3b). This may be ascribed to the relatively more consistent urban development trajectories among sub-provincial cities, as controlled by factors such as similar geographical conditions and accordant governance in steering climate-conscious urban development. Besides, it may also be partly contributed by its less variability of background climatic conditions (Fig. 3a).

More specifically, in addition to the impacts of climatic backgrounds, the regional discrepancy may be directly related to the diversified characteristics of urban development across China, for instance, the uneven urban expansion (Tan and Li, 2015; Li et al., 2017) and the associated landscape and socio-economic differences (Yao et al., 2017) between old and new urban areas. Here, we cast a glance at the linkage between the LST difference (Fig. 3a) and the selected indictors (Fig. 4). Apparently, the large cities in the North China Plain exhibiting noticeably

"cooler" new urban areas are largely located in the warm temperature zone characterized with moderate temperature conditions across China. They are generally associated with more vegetation coverage (Fig. 4a) and less socio-economic activities (Fig. 4e-f) in these areas, and also higher levels of urban land agglomeration (Fig. 4b) for the whole city. While the numerous cooler cities in western China showing evidently "hotter" new urban areas (Fig. 3a) are mainly small-sized with remarkable expansion rates (Fig. 2a), which may be partly a product of policy invention since the early 1990s (Section 2.1). The emerging "hotter" new urban areas for these fast-growing small cities highlight the injustice of most existing studies to only focus on larger cities in China while exploring the thermal environmental impacts of urban expansion (Wang et al., 2015; Zhou et al., 2014, 2016; Yao et al., 2017). In fact, small Asian cities, one of the most under-represented segments (divided according to region and city size across the globe) in urban climate studies, are projected to share the largest proportion of global urban population by 2030 (Lamb et al., 2019). Hence, it is urgent to generate comprehensive knowledge of urbanization-temperature interactions for these small cities, so that decision-makers can develop strategies to cope with the existing urban heat problems and steer the future massive urban expansion into more climate-friendly.

4.2. Impacts of urban development on the LST difference

MGWR further reveals the relationships between LST difference and the selected urban development indicators to operate at diverse spatial scales. Overall, four different operating scales are identified, including three local scales for urban elevation difference, NDVI difference, and Gini coefficient (Table 2; Fig. 5), and a global scale for EUR, Moran's I, GDP and population densities (Table 2). Such a result, on one hand, endorses the superiority of MGWR in simultaneously capturing both spatial non-stationarity and scale-dependence of geographical processes. On the other hand, it indicates that, in addition to the observational scale investigated in previous studies (Luan et al., 2020), operational scale is also an important issue to be considered in investigating the urbanization-temperature relationship. In fact, the significance of scale has been extensively emphasized in all sciences (Levin, 1992; Sayre, 2005, 2009), especially in geographical contexts (Goodchild, 2001, 2004; Fotheringham et al., 2017; Murakami et al., 2018). Nature and human systems are simultaneously controlled by numerous processes operating on multiple spatial scales (Turner et al., 1989; Levin, 1992; Sayre, 2005, 2009), so is the human-environment interactions as explored in this study. Overall, the scale-dependent feature of the processes enables us a better understanding of the urban development-LST difference relationships. Besides, those relationships operating at local scales can also help decision-makers in generating geographically targeted references, so as to mitigate local surface warming and minimize intra-urban thermal variation.

Specifically, for the three relationships operating at local scales, the spatially varying patterns can be attributed to the diversified land surface characteristics regulated by non-uniform urban development patterns and complex natural environments. For instance, the spatially varying impacts of the NDVI difference (Fig. 5a) may be collectively induced by diversified urban greenery characteristics and complex background climatic conditions. On one hand, the cooling effect of vegetation is locally controlled by its land surface properties of type, size and shape (Ouyang et al., 2020; Yu et al., 2020), and also the irrigation regime (Spronken-Smith and Oke, 1998), which cannot be fully captured by any single vegetation indicator, such as NDVI. Therefore, the other properties of vegetation neglected by NDVI would give rise to a spatially varying cooling effect. On the other hand, the cooling effect is also regulated by macroscopic climatic backgrounds (Spronken-Smith and Oke, 1998; Manoli et al., 2019; Martilli et al., 2020). For instance, governed by physical mechanisms such as the increase in vapor pressure deficit, well irrigated vegetation can be more effective in cooling urban areas in dry climates compared to humid ones (Yu et al., 2018; Manoli et al., 2019; Martilli et al., 2020). Hence, in this study, a stronger negative impact of NDVI difference (Fig. 5a) is captured for the majority of cities located in West China where the climate is generally characterized with low precipitation (Song et al., 2019). The spatially varying impact of the old-new elevation difference (Fig. 5b, c) may also be conjointly contributed by multiple factors. For instance, the differentiated amount of solar radiation received in different climate zones, the other topographical characteristics (i.e., slope and aspect) (Peng et al., 2020) not covered in this study, and also the diversified urban ventilation conditions partly regulated by complex urban topography (Kitous et al., 2012; He et al., 2020). In regard to the Gini coefficient, in contrast to the globally consistent impact of the global Moran's I, it correlates with the LST difference in a spatially varying manner. Such a spatially inconsistent impact on the LST difference may be largely a consequence of the differentiated spatial patterns of urban areas under identical inequality levels of landscape urbanization.

The significant impact of elevation on the "cooler" new urban areas, as revealed by MGWR, sheds new light on our understanding of the urbanization-temperature relationship. First, it highlights the limitations of previous studies in ignoring the influence of topography and simply ascribing the descending trends of SUHII to the improved urban greenery management (Zhou et al., 2016; Liu et al., 2020) or lower development intensity (Zhou et al., 2016). That is to say, the neglect of nature-driven influence, such as elevation, will lead to overestimation of the efficacy of human-driven interventions in mitigating urban heat problems and facilitating urban sustainability. In fact, higher elevation is significantly correlated with lower LST (Khandelwal et al., 2018; Peng et al., 2020). It also normally acts as a restrictive factor to urban expansion (Li et al., 2018). Nevertheless, unlike the old urban areas, new urban areas can be built at higher elevation with sufficient financial support and technology innovation (Dubovyk et al., 2011; Li et al., 2018) and thus revealing relatively lower LSTs. Second, the significant impact of elevation also indicates that, it is crucial for LST/ SUHI projections under future urban development scenarios to take into account the variation of elevation, which has been largely ignored in previous efforts using statistical models (Huang et al., 2019). Third, compared to previous studies showing non-significant impact of topography on SUHI based on limited city samples (Zhou et al., 2014), the contrary finding revealed in this study endorses the superiority of using large city samples in investigating the urbanization-temperature relationship.

The contrary relationships between LST difference and the GDP and population indicators (Table 2) also highlight the complexity of urban systems. Generally, higher LST tends to occur in urban areas characterized with relatively higher population density but lower economic levels. This indicates that the evolving urban dynamics have brought about a complex coupling relationship among LST, local social status, and economic levels. Previous studies have ascribed such a complex relationship to the LC modification induced by the urbanization process, primarily in terms of vegetation cover and building density (Jenerette et al., 2007; Huang and Cadenasso, 2016). Specifically, large population always comes along with intense urban development and limited space for urban greening, thus undoubtedly leading to an elevated LST (Jenerette et al., 2007; Huang and Cadenasso, 2016; Peng et al., 2018). Besides, it is also associated with more anthropogenic heat release which further intensifies the local urban heat problems (Yin et al., 2018; Yang et al., 2019b; Chen et al., 2020). As for the urban areas with superior economic conditions (higher incomes), they are intrinsically correlated with more vegetation cover and thus decreased LST levels (Jenerette et al., 2007; Huang and Cadenasso, 2016).

4.3. Implications and limitations

The old-new LST variation indicates that cities are facing both opportunities and challenges for urban sustainability. On one hand, the emerging "cooler" new urban areas confirm the great possibility of

facilitating climate-conscious urban development through urban governance. For instance, to implement more stringent urban greening policies in newly expanded urban areas. Taking Beijing as an example, the relatively "cooler" new urban areas (Fig. 3a) can be partly attributed to its regulation issued in 2010 requiring the proportion of vegetation cover to be no less than 30% in all newly built residential areas (Wang et al., 2019a). In fact, the more abundant vegetation in new urban areas is observed in 92% of the cities across China (Fig. 4a), which may be collectively contributed by the favorable nature endowment and also positive policy-driven interventions. In the future, knowledge of urban climate science can be progressively translated into decision-making through approaches such as spatial planning and urban design (Mills et al., 2010; Georgescu et al., 2014). Hence, the massive urban land projected in the future, especially in Africa and Asia (Gao and O'Neill, 2020), can be steered into more climate-friendly. It is noteworthy that, behind the "cooler" new urban environment, there is usually lower development density associating with longer commuting distances (Yue et al., 2019), and thus increased greenhouse gas (GHG) emissions (Cremades and Sommer, 2019) and ultimately elevated climate warming on the global scale. Hence, an integrated policy framework is urgently needed to incorporate local warming mitigation with GHG emission restriction, so that synergies rather than trade-offs between the two aspects can be possibly maximized (Ürge-vorsatz et al., 2018). Furthermore, we may achieve the 13th Sustainable Development Goal (climate action) emphasized in the 2030 Agenda for Sustainable Development (Fuso Nerini et al., 2019).

On the other hand, the relatively "hotter" old urban areas also indicate that the population living or working there (Fig. 4f) is exposed to more severe urban heat problems, especially for the numerous cities located in the warm temperature zone (Fig. 3a; 3d). The elevated LST would compel the urban dwellers into higher threat of human health, especially during heat waves (Patz et al., 2005). Such a thermal inequality emphasizes the necessity to minimize intra-urban thermal environmental inequality and more efforts should be made to cool the relatively "hotter" old urban areas for the vast majority of cities in China. Nevertheless, old urban areas are usually high-density areas with limited heat-adaptive capacity, thus demanding more detailed and flexible policies, such as vertical greenery (green facades and green roofs) (He, 2019; Liu et al., 2020) and "Plant Where Possible" (Wang et al., 2019a). For instance, the urban renewal projects in Shanghai has successfully embedded scattered green patches among the high-rise buildings since 2005, thus effectively attenuated the heat stress in old urban centers (Wang and Shu, 2020) and reduced its old-new LST difference (Figs. 3a, 4a).

The spatially varying impacts of the selected indicators on the LST difference, especially for the NDVI difference, can provide geographically targeted references for mitigating local surface warming and minimizing intra-urban thermal variation. For instance, the relatively weaker cooling, and even warming effect of vegetation as observed in humid areas, including south central and northeast China (Fig. 5a), necessitate more stringent urban greenery planning and management for these areas. Namely, be cautious with the type, size, shape, connectivity, and complexity of green spaces so as to achieve the best cooling effect (Yu et al., 2020). This is especially true for northeast China where higher LSTs tend to occur in old urban areas (Fig. 3a) which are normally with limited heat-adaptive capacity. Generally, tree-covered urban green vegetation can be a recommendable effective approach (Yu et al., 2018, 2020). While for the western cities characterized by dry climate, the stronger cooling effect of vegetation (Fig. 5a) denotes that we may be able to apply less urban green space to achieve the optimal cooling effect, as long as water supply can be guaranteed for irrigation (Yu et al., 2020). As for the impacts of elevation, it is noteworthy that, northeast and central China experience stronger influences. Hence, it is essential for studies targeted on these areas to cover elevation into consideration while investigating the contributors of surface local warming or projecting LST/ SUHI under future urban development scenarios. The spatially varying impacts of the Gini coefficient also indicate that, generally northern cities should be more concerned about landscape urbanization inequality to minimize intra-urban thermal variation.

There are also several aspects that may be improved in future work. First, uncertainties exist in the identification of old and new urban areas. This study employs a competitive LC product, the widely used ESA-CCI LC (300-m-resolution), to identify the urban areas for 1992 and 2015. Nevertheless, LC datasets generated by different data sources with diversified resolutions may derive urban areas with certain discrepancies. Second, the selected seven indicators interpret 75% of the variance in the LST difference through MGWR, nevertheless, they are still insufficient to depict the complex and geographically variable urban systems. Urban expansion is associated with the evolution of urban development in terms of both urban form and urban function. The evolution varies from the materials used in construction to development priorities. Hence, in the future, more detailed and comprehensive indicators depicting the complete picture of urban systems should be involved. For instance, we may directly use the indicator of anthropogenic heat emission (Chen et al., 2020; Wang et al., 2020), other than its socio-economic drivers, to investigate the urban development-surface thermal environment relationship. Third, this study focuses on the daytime patterns using annually averaged daytime LST data, nevertheless, the LST difference and the corresponding relationships with influencing factors might vary both diurnally and seasonally. Therefore, future works can be devoted to investigate the diurnal and seasonal patterns of the LST difference and the old-new thermal inequality reshaped by the diurnal population dynamics.

5. Conclusion

This study provides the first attempt to capture the intra-urban variation of surface thermal environment triggered by significant urban dynamics on large scales. The main findings can be summarized as follows: (1) urban development is closely accompanied by the presence of intra-urban LST difference between conventional old urban centers and newly expanded urban areas in Chinese cities. The LST difference varies significantly across China, and 82% of the cities manifest relatively "cooler" urban environments in the generally larger-sized new urban areas. (2) The selected indicators can interpret 75% of the variance in the LST difference through MGWR. Among them, the old-new urban elevation difference, NDVI difference, and Gini coefficient, which rank as the three leading influential indicators, exhibit spatially varying relationships with the LST difference across China, thus endorsing the superiority of MGWR in capturing multi-scale spatial heterogeneity in environmental responsive processes. Specifically, the elevation difference, which has been largely neglected or underestimated in long-term trend analysis of LST/SUHII, is found dominant in explaining the LST difference for 252 cities (78%), among which 216 cities demonstrate higher LSTs in the urban areas with lower elevations. In contrast, the less evident relationships with UER, Moran's I, and the old-new differences of GDP and population densities are globally consistent. Overall, the findings provide valuable generalized information for climatic modelling and temperature projection. The city-specific characteristics investigated in this study can also benefit all-sized cities in China in developing urban heat mitigation strategies. In the future, more efforts can be devoted to digging the underlying mechanism of the old-new LST difference using more sophisticated indicator system, and assessing both the diurnal and seasonal patterns of the old-new thermal inequality.

CRediT authorship contribution statement

Huimin Liu: Conceptualization, Data curation, Formal analysis, Investigation, Methodology, Validation, Visualization, Writing - original draft preparation. **Bo Huang**: Conceptualization, Funding acquisition,

Resources, Supervision, Writing - review & editing. **Sihang Gao**: Formal analysis, Investigation, Software, Visualization. **Jiong Wang**: Investigation, Writing - review & editing. **Chen Yang**: Data curation, Formal analysis, Software. **Rongrong Li**: Data curation, Writing - review & editing.

Declaration of competing interest

The authors declare that they have no known competing financial interests or personal relationships that could have appeared to influence the work reported in this paper.

Acknowledgments

This research was supported by the Strategic Priority Research Program of the Chinese Academy of Sciences (Grant No. XDA19090108) and the Impact Postdoctoral Fellowship Scheme of the Chinese University of Hong Kong (CUHK) 2019. The authors also thank the editor and the four anonymous reviewers for their insightful comments that have been very helpful in improving this paper.

Appendix A. Supplementary data

Supplementary data to this article can be found online at https://doi.org/10.1016/j.scitotenv.2020.144810.

References

Anselin, L., 2010. Thirty years of spatial econometrics. Pap. Reg. Sci. 89, 3–25. https://doi.org/10.1111/j.1435-5957.2010.00279.x.

Anselin, L., Syabri, I., Kho, Y., 2006. GeoDa: an introduction to spatial data analysis. Geograph Anal 38, 5–22. https://doi.org/10.1111/j.0016-7363.2005.00671.x.

Bendel, R.B., Higgins, S.S., Pyke, D.A., 1989. Comparison of skewness coefficient, coefficient of variation, and gini coefficient as inequality measures within populations. Oecologia 78, 394–400. https://doi.org/10.1007/BF00379115.

Chai, B., Seto, K.C., 2019. Conceptualizing and characterizing micro-urbanization: a new perspective applied to Africa. Landsc. Urban Plan. 190, 103595. https://doi.org/10.1016/j.landurbplan.2019.103595.

Chen, Q., Yang, X., Ouyang, Z., Zhao, N., Jiang, Q., Ye, T., Qi, J., Yue, W., 2020. Estimation of anthropogenic heat emissions in China using cubist with points-of-interest and multisource remote sensing data. Environ. Pollut. 266, 115183. https://doi.org/10.1016/j.envpol.2020.115183.

Clinton, N., Gong, P., 2013. MODIS detected surface urban heat islands and sinks: global locations and controls. Remote Sens. Environ. 134, 294–304. https://doi.org/10.1016/j.rse.2013.03.008.

Cremades, R., Sommer, P.S., 2019. Computing climate-smart urban land use with the integrated urban complexity model (IUCm 1.0). Geosci. Model Dev. 12, 525–539. https://doi.org/10.5194/gmd-12-525-2019.

Dubovyk, O., Sliuzas, R., Flacke, J., 2011. Spatio-temporal modelling of informal settlement development in Sancaktepe district, Istanbul. Turkey. ISPRS J. Photogramm. Remote Sens. 66, 235–246. https://doi.org/10.1016/j.isprsjprs.2010.10.002.

ESA, 2015. Climate Change Initiative of the European Space Agency (ESA-CCI). http://maps.elie.ucl.ac.be/CCI/.

ESA, 2018. Land Cover CCI Product User Guide Version, 2.0 available at:. http://maps.elie.ucl.ac.be/CCI/viewer/download/ESACCI-LC-Ph2-PUGv2_2.0.pdf.

Esch, T., Heldens, W., Hirne, A., Keil, M., Marconcini, M., Roth, A., Zeidler, J., Dech, S., Strano, E., 2017. Breaking new ground in mapping human settlements from space – the global urban footprint. ISPRS J. Photogramm. Remote Sens. 134, 30–42. https://doi.org/10.1016/j.isprsjprs.2017.10.012.

Estrada, F., Botzen, W.J.W., Tol, R.S.J., 2017. A global economic assessment of city policies to reduce climate change impacts. Nat. Clim. Chang. 7, 403–406. https://doi.org/10.1038/nclimate3301.

Fan, C., Myint, S., 2014.A comparison of spatial autocorrelation indices and landscape metrics in measuring urban landscape fragmentation. Landsc. Urban Plan. 121, 117–128. doi:https://doi.org/10.1016/j.landurbplan.2013.10.002.

Finley, A.O., 2011. Comparing spatially-varying coefficients: models for analysis of ecological data with non-stationarity and anisotropic residual dependence. Methods Ecol. Evol. 2, 143–154. https://doi.org/10.1111/j.2041-210X.2010.00060.x.

Foley, J.A., Defries, R., Asner, G.P., Barford, C., Bonan, G., Carpenter, S.R., Stuart Chapin, F., Coe, M.T., Daily, G.C., Gibbs, H.K., Helkowski, J.H., Holloway, Tracey, Howard, E.A., Kucharik, C.J., Monfreda, Chad, Patz, J.A., Colin Prentice, I., Ranmankutty, Navin, Snyder, P.K., 2005. Global consequences of land use. Science 309, 570–574. https://doi.org/10.1126/science.1111772.

Fotheringham, A.S., Brunsdon, C., Charlton, M., 2002. Geographically Weighted Regression—The Analysis of Spatially Varying Relationships. John Wiley & Sons Ltd., West Sussex, UK.

Fotheringham, A.S., Yang, W., Kang, W., 2017. Multiscale geographically weighted regression (MGWR). Ann. Am. Assoc. Geogr. 107, 1247–1265. https://doi.org/10.1080/24694452.2017.1352480.

Fu, Y., Li, J., Weng, Q., Zheng, Q., Li, L., Dai, S., Guo, B., 2019. Characterizing the spatial pattern of annual urban growth by using time series Landsat imagery. Sci. Total Environ. 666, 274–284. https://doi.org/10.1016/j.scitotenv.2019.02.178.

Fuso Nerini, F., Sovacool, B., Hughes, N., Cozzi, L., Cosgrave, E., Howells, M., Tavoni, M., Tomei, J., Zerriffi, H., Milligan, B., 2019. Connecting climate action with other sustainable development goals. Nat. Sustain. 2, 674–680. https://doi.org/10.1038/s41893-019-0334-y.

Gao, J., O'Neill, B.C., 2020. Mapping global urban land for the 21st century with data-driven simulations and shared socioeconomic pathways. Nat. Commun. 11, 2302. https://doi.org/10.1038/s41467-020-15788-7.

Georgescu, M., Morefield, P.E., Bierwagen, B.G., Weaver, C.P., 2014. Urban adaptation can roll back warming of emerging megapolitan regions. Proc. Natl. Acad. Sci. 111, 2909–2914. https://doi.org/10.1073/pnas.1322280111.

Goodchild, M. Models of scale and scales of modelling. In Modelling Scale in Geographic Information Science; Tate, N., Atkinson, P.M., Eds.; Wiley: Chichester, UK, 2001; pp. 3–10.

Goodchild, M.F., 2004. The validity and usefulness of laws in geographic information science and geography. Ann. Assoc. Am. Geogr. 94, 300–303. https://doi.org/10.1111/j.1467-8306.2004.09402008.x.

Grimm, N.B., Faeth, S.H., Golubiewski, N.E., Redman, C.L., Wu, J., Bai, X., Briggs, J.M., 2008. Global change and the ecology of cities. Science 319, 756. https://doi.org/10.1126/science.1150195.

GSD, 2015. Geospatial Data Cloud site. Computer Network Information Center, Chinese Academy of Sciences (GSD) http://www.gscloud.cn.

Güneralp, B., Reba, M., Hales, B.U., Wentz, E.A., Seto, K.C., 2020. Trends in urban land expansion, density, and land transitions from 1970 to 2010: a global synthesis. Environ. Res. Lett. 15, 044015. https://doi.org/10.1088/1748-9326/ab6669.

He, B., Ding, L., Prasad, D., 2020. Relationships among local-scale urban morphology, urban ventilation, urban heat island and outdoor thermal comfort under sea breeze influence. Sustain. Cities Soc. 60, 102289. https://doi.org/10.1016/j.scs.2020.102289.

He, B.J., 2019. Towards the next generation of green building for urban heat island mitigation: zero UHI impact building. Sustain. Cities Soc. 101647. https://doi.org/10.1016/j.scs.2019.101647.

Huang, G.L., Cadenasso, M.L., 2016. People, landscape, and urban heat island: dynamics among neighborhood social conditions, land cover and surface temperatures. Landsc. Ecol. 31, 2507–2515. https://doi.org/10.1007/s10980-016-0437-z.

Huang, K., Li, X., Liu, X., Seto, K.C., 2019. Projecting global urban land expansion and heat island intensification through 2050. Environ. Res. Lett. 14, 114037. https://doi.org/10.1088/1748-9326/ab4b71.

Imhoff, M.L., Zhang, P., Wolfe, R.E., Bounoua, L., 2010. Remote sensing of the urban heat island effect across biomes in the continental USA. Remote Sens. Environ. 114, 504–513. https://doi.org/10.1016/j.rse.2009.10.008.

Jenerette, G.D., Harlan, S.L., Brazel, A., Jones, N., Larsen, L., Stefanov, W.L., 2007. Regional relationships between surface temperature, vegetation, and human settlement in a rapidly urbanizing ecosystem. Landsc. Ecol. 22, 353–365. https://doi.org/10.1007/s10980-006-9032-z.

Jia, W., Zhao, S., 2020. Trends and drivers of land surface temperature along the urban-rural gradients in the largest urban agglomeration of China. Sci. Total Environ. 711, 134579. https://doi.org/10.1016/j.scitotenv.2019.134579.

Khandelwal, S., Goyal, R., Kaul, N., Mathew, A., 2018. Assessment of land surface temperature variation due to change in elevation of area surrounding Jaipur. India. Egypt. J. Remote Sens. Space Sci. 21, 87–94. https://doi.org/10.1016/j.ejrs.2017.01.005.

Kitous, S., Bensalem, R., Adolphe, L., 2012. Airflow patterns within a complex urban topography under hot and dry climate in the Algerian Sahara. Build. Environ. 56, 162–175. https://doi.org/10.1016/j.buildenv.2012.02.022.

Lamb, W.F., Creutzig, F., Callaghan, M.W., Minx, J.C., 2019. Learning about urban climate solutions from case studies. Nat. Clim. Chang. 9, 279–287. https://doi.org/10.1038/s41558-019-0440-x.

Lemoine-Rodríguez, R., Inostroza, L., Zepp, H., 2020. The global homogenization of urban form. An assessment of 194 cities across time. Landsc. Urban Plan. 204, 103949. doi: https://doi.org/10.1016/j.landurbplan.2020.103949.

Levin, S.A., 1992. The problem of pattern and scale in ecology. Ecol. Time Ser. 73, 277–326. http://www.jstor.org/stable/1941447.

Li, D., Liao, W., Rigden, A.J., Liu, X., Wang, D., Malyshev, S., Shevliakova, E., 2019. Urban heat island: aerodynamics or imperviousness? Sci. Adv. 5, eaau4299. doi:https://doi.org/10.1126/sciadv.aau4299.

Li, G., Sun, S., Fang, C., 2018. The varying driving forces of urban expansion in China: insights from a spatial-temporal analysis. Landsc. Urban Plan. 174, 63–77. https://doi.org/10.1016/j.landurbplan.2018.03.004.

Li, S., Zhao, Z., Miaomiao, X., Wang, Y., 2010. Investigating spatial non-stationary and scale-dependent relationships between urban surface temperature and environmental factors using geographically weighted regression. Environ. Model. Softw. 25, 1789–1800. https://doi.org/10.1016/j.envsoft.2010.06.011.

Li, X., Zhou, Y., Asrar, G.R., Imhoff, M., Li, X., 2017. The surface urban heat island response to urban expansion: a panel analysis for the conterminous United States. Sci. Total Environ. 605–606, 426–435. https://doi.org/10.1016/j.scitotenv.2017.06.229.

Li, Y., Schubert, S., Kropp, J.P., Rybski, D., 2020. On the influence of density and morphology on the urban heat island intensity. Nat. Commun. 11, 2647. https://doi.org/10.1038/s41467-020-16461-9.

Liu, H., Zhan, Q., Yang, C., Wang, J., 2019a. The multi-timescale temporal patterns and dynamics of land surface temperature using ensemble empirical mode decomposition. Sci. Total Environ. 652, 243–255. https://doi.org/10.1016/j.scitotenv.2018.10.252.

Liu, H., Zhan, Q., Gao, S., Yang, C., 2019b. Seasonal variation of the spatially non-stationary association between land surface temperature and urban landscape. Remote Sens. 11, 1016. https://doi.org/10.3390/rs11091016.
Liu, H., Huang, B., Yang, C., 2020. Assessing the coordination between economic growth and urban climate change in China from 2000 to 2015. Sci. Total Environ. 732, 139283. https://doi.org/10.1016/j.scitotenv.2020.139283.
Liu, Y., Peng, J., Wang, Y., 2018. Efficiency of landscape metrics characterizing urban land surface temperature. Landsc. Urban Plan. 180, 36–53. https://doi.org/10.1016/j.Landurbplan.2018.08.006.
Long, Y., Zhai, W., Shen, Y., Ye, X., 2018. Understanding uneven urban expansion with natural cities using open data. Landsc. Urban Plan. 177, 281–293. https://doi.org/10.1016/j.landurbplan.2017.05.008.
Luan, X., Yu, Z., Zhang, Y., Wei, S., Miao, X., Huang, Z.Y.X., Teng, S.N., Xu, C., 2020. Remote sensing and social sensing data reveal scale-dependent and system-specific strengths of urban heat island determinants. Remote Sens. 12, 391. https://doi.org/10.3390/rs12030391.
Manoli, G., Fatichi, S., Schläpfer, M., Yu, K., Crowther, T.W., Meili, N., Burlando, P., Katul, G.G., Bou-Zeid, E., 2019. Magnitude of urban heat islands largely explained by climate and population. Nature 573, 55–60. https://doi.org/10.1038/s41586-019-1512-9.
Martilli, A., Roth, M., Chow, W. T., Demuzere, M., Lipson, M., Krayenhoff, E. S., Sailor, D., Nazarian, N., Voogt, J., Wouters, H., Middel, A., Stewart, I.D., Bechtel, B., Christen, A., Hart, M.A., 2020. Summer Average Urban-rural Surface Temperature Differences Do Not Indicate the Need for Urban Heat Reduction. doi:10.31219/osf.io/8gnbf.
Mills, G., Cleugh, H., Emmanuel, R., Endlicher, W., Erell, E., Mc Granahan, G., Ng, E., Nickson, A., Rosenthal, J., Steemer, K., 2010. Climate information for improved planning and management of mega cities (needs perspective). Procedia Environ. Sci. 1, 228–246. https://doi.org/10.1016/j.proenv.2010.09.015.
Murakami, D., Lu, B., Harris, P., Brunsdon, C., Charlton, M., Nakaya, T., Griffith, D.A., 2018. The importance of scale in spatially varying coefficient modeling. Ann. Am. Assoc. Geogr. 109, 50–70. https://doi.org/10.1080/24694452.2018.1462691.
NBSC (1979-2019), 2019. China City Statistical Yearbook. China Statistical Press, Beijing various years. http://www.stats.gov.cn/.
NBSC (National Bureau of Statistics of China), 2016. China City Statistical Yearbook. China Statistical Press, Beijing http://www.stats.gov.cn/.
Oke, T.R., 1973. City size and the urban heat island. Atmos. Environ. 7, 769–779. https://doi.org/10.1016/0004-6981(73)90140-6.
Oke, T.R., Mills, G., Christen, A., Voogt, J.A., 2017. Urban Climates. Cambridge University Press, Cambridge, UK.
Ouyang, W., Morakinyo, T.E., Ren, C., Ng, E., 2020. The cooling efficiency of variable greenery coverage ratios in different urban densities: a study in a subtropical climate. Build. Environ. 174, 106772. https://doi.org/10.1016/j.buildenv.2020.106772.
Patz, J.A., Campbell-Lendrum, D., Holloway, T., Foley, Jonathan A., 2005. Impact of regional climate change on human health. Nature 438, 310–317. https://doi.org/10.1038/nature04188.
Peng, J., Jia, J., Liu, Y., Li, H., Wu, J., 2018. Seasonal contrast of the dominant factors for spatial distribution of land surface temperature in urban areas. Remote Sens. Environ. 215, 255–267. https://doi.org/10.1016/j.rse.2018.06.010.
Peng, S., Piao, S., Ciais, P., Friedlingstein, P., Ottle, C., Bréon, F.-M., Nan, H., Zhou, L., Myneni, R.B., 2011. Surface urban heat island across 419 global big cities. Environ. Sci. Technol. 46, 696–703. https://doi.org/10.1021/es2030438.
Peng, X., Wu, W., Zheng, Y., Sun, J., Hu, T., Wang, P., 2020. Correlation analysis of land surface temperature and topographic elements in Hangzhou, China. Sci. Rep. 10, 10451. https://doi.org/10.1038/s41598-020-67423-6.
Pesaresi, M., Ehrlich, D., Ferri, S., Florczyk, A.J., Freire, S., Halkia, S., Julea, A.M., Kemper, T., Soille, P., Syrris, V., 2016. Operating Procedure for the Production of the Global Human Settlement Layer From Landsat data of the Epochs 1975, 1990, 2000, and 2014. Luxembourg: Publications Office of the European Union, EUR 27741 EN.
RESDC, 2015. Data Center for Resources and Environmental Sciences, Chinese Academy of Sciences (RESDC). http://www.resdc.cn.
Sayre, N.F., 2005. Ecological and geographical scale: parallels and potential for integration. Prog. Hum. Geogr. 29, 276–290. https://doi.org/10.1191/0309132505ph546oa.
Sayre, N.F., 2009. Scale. A Companion to Environmental Geography, Edited by: Castree, N., Demeritt, D., Liverman, D. Rhoads, B. Blackwell Publishing, Malden, MA, pp. 95–108 https://doi.org/10.1002/9781444305722.ch7.
Seto, K.C., Golden, J.S., Alberti, M., 2017. Sustainability in an urbanizing planet. Proc. Natl. Acad. Sci. U. S. A. 114, 8935–8938. https://doi.org/10.1073/pnas.1606037114.
Song, Y., Chen, B., Kwan, M.P., 2019. How does urban expansion impact people's exposure to green environments? A comparative study of 290 Chinese cities. J. Clean. Prod. 246, 119018. https://doi.org/10.1016/j.jclepro.2019.119018.
Spronken-Smith, R.A., Oke, T.R., 1998. The thermal regime of urban parks in two cities with different summer climates. Int. J. Remote Sens. 19, 2085–2104. https://doi.org/10.1080/014311698214884.
Stewart, I., Oke, T., January 2009. Newly developed "thermal climate zones" for defining and measuring urban heat island magnitude in the canopy layer. In Proceedings of the Eighth Symposium on Urban Environment, Phoenix, AZ, USA, pp. 11–15.
Stone, B., 2012. The City and the Coming Climate: Climate Change in the Places We Live. Cambridge University Press, New York.
Su, Y.-F., Foody, G.M., Cheng, K.-S., 2012. Spatial non-stationarity in the relationships between land cover and surface temperature in an urban heat island and its impacts on thermally sensitive populations. Landsc. Urban Plan. 107, 172–180. https://doi.org/10.1016/j.landurbplan.2012.05.016.
Sun, R., Xie, W., Chen, L., 2018. A landscape connectivity model to quantify contributions of heat sources and sinks in urban regions. Landsc. Urban Plan. 178, 43–50. https://doi.org/10.1016/j.landurbplan.2018.05.015.
Tan, M., Li, X., 2015. Quantifying the effects of settlement size on urban heat islands in fairly uniform geographic areas. Habitat. Int. 49, 100–106. https://doi.org/10.1016/j.habitatint.2015.05.013.
Turner, M.G., Dale, V.H., Gardner, R.H., 1989. Predicting across scales: theory development and testing. Landsc. Ecol. 3, 245–252. https://doi.org/10.1007/BF00131542.
Ürge-vorsatz, D., Rosenzweig, C., Dawson, R.J., Rodriguez, R.S., Bai, X., Barau, A.S., Seto, K.C., Dhakal, S., 2018. Locking in positive climate responses in cities. Nat. Clim. Chang. 8, 174–177. https://doi.org/10.1038/s41558-018-0100-6.
Wan, Z., 2008. New refinements and validation of the MODIS land-surface temperature/emissivity products. Remote Sens. Environ. 112, 59–74. https://doi.org/10.1016/j.rse.2006.06.026.
Wang, C., Li, Y., Myint, S.W., Zhao, Q., Wentz, E.A., 2019b. Impacts of spatial clustering of urban land cover on land surface temperature across Köppen climate zones in the contiguous United States. Landsc. Urban Plan. 192, 103668. https://doi.org/10.1016/j.landurbplan.2019.103668.
Wang, J., Huang, B., Fu, D., Atkinson, P.M., 2015. Spatiotemporal variation in surface urban heat island intensity and associated determinants across major Chinese cities. Remote Sens. 7, 3670–3689. https://doi.org/10.3390/rs70403670.
Wang, J., Zhou, W., Wang, J., 2019a. Time-series analysis reveals intensified urban heat island effects but without significant urban warming. Remote Sens. 11, 2229. https://doi.org/10.3390/rs11192229.
Wang, S., Hu, D., Yu, C., Chen, S., Di, Y., 2020. Mapping China's time-series anthropogenic heat flux with inventory method and multi-source remotely sensed data. Sci. Total Environ. 734, 139457. https://doi.org/10.1016/j.scitotenv.2020.139457.
Wang, W., Shu, J., 2020. Urban renewal can mitigate urban heat islands. Geophys. Res. Lett. 47, 6. https://doi.org/10.1029/2019GL085948.
Wei, Y., 1994. Urban policy, economic policy, and the growth of large cities in China. Habitat. Int. 18, 53–65. https://doi.org/10.1016/0197-3975(94)90017-5.
Wei, Y.D., 2015. Spatiality of regional inequality. Appl. Geogr. 61, 1–10. https://doi.org/10.1016/j.apgeog.2015.03.013.
Wu, J., Xiang, W., Zhao, J., 2014. Urban ecology in China: historical developments and future directions. Landsc. Urban Plan. 125, 222–233. https://doi.org/10.1016/j.landurbplan.2014.02.010.
Yang, B., Yang, X., Leung, L.R., Zhong, S., Qian, Y., Zhao, C., Chen, F., Zhang, Y., Qi, J., 2019b. Modeling the impacts of urbanization on summer thermal comfort: the role of urban land use and anthropogenic heat. J. Geophys. Res. Atmos. 124, 6681–6697. https://doi.org/10.1029/2018JD029829.
Yang, C., Zhan, Q., Lv, Y., Liu, H., 2019a. Downscaling land surface temperature using multiscale geographically weighted regression over heterogeneous landscapes in Wuhan. China. IEEE J. Sel. Topics Appl. Earth Observ. Remote Sens. 12, 5213–5222. https://doi.org/10.1109/JSTARS.2019.2955551.
Yao, R., Wang, L., Huang, X., Niu, X., Liu, F., Wang, Q., 2017. Temporal trends of surface urban heat islands and associated determinants in major Chinese cities. Sci. Total Environ. 609, 742–754. https://doi.org/10.1016/j.scitotenv.2017.07.217.
Ye, J.A., Xu, J., Yi, H., 2006. The fourth wave of urbanization in China. City Planning Review 30, 13–18.
Yin, C., Yuan, M., Lu, Y., Huang, Y., Liu, Y., 2018. Effects of urban form on the urban heat island effect based on spatial regression model. Sci. Total Environ. 634, 696–704. https://doi.org/10.1016/j.scitotenv.2018.03.350.
Yu, Z., Xu, S., Zhang, Y., Jørgensen, G., Vejre, H., 2018. Strong contributions of local background climate to the cooling effect of urban green vegetation. Sci. Rep. 8, 6798. https://doi.org/10.1016/10.1038/s41598-018-25296-w.
Yu, Z., Yang, G., Zuo, S., Jørgensen, G., Koga, M., Vejre, H., 2020. Critical review on the cooling effect of urban blue-green space: a threshold-size perspective. Urban For. Urban Green. 49, 126630. https://doi.org/10.1016/j.ufug.2020.126630.
Yue, W., Liu, X., Zhou, Y., Liu, Y., 2019. Impacts of urban configuration on urban heat island: an empirical study in China megacities. Sci. Total Environ. 671, 1036–1046. https://doi.org/10.1016/j.scitotenv.2019.03.421.
Zhao, C., Jensen, J., Weng, Q., Weaver, R., 2018. A geographically weighted regression analysis of the underlying factors related to the surface urban heat island phenomenon. Remote Sens. 10, 1428. https://doi.org/10.3390/rs10091428.
Zhou, B., Rybski, D., Kropp, J.P., 2013. On the statistics of urban heat island intensity. Geophys. Res. Lett. 40, 5486–5491. https://doi.org/10.1002/2013GL057320.
Zhou, B., Rybski, D., Kropp, J.P., 2017. The role of city size and urban form in the surface urban heat island. Sci. Rep. 7, 4791. https://doi.org/10.1038/s41598-017-04242-2.
Zhou, D., Zhao, S., Liu, S., Zhang, L., Zhu, C., 2014. Surface urban heat island in China's 32 major cities: spatial patterns and drivers. Remote Sens. Environ. 152, 51–61. https://doi.org/10.1016/j.rse.2014.05.017.
Zhou, D., Zhang, L., Hao, L., Sun, G., Liu, Y., Zhu, C., 2016. Spatiotemporal trends of urban heat island effect along the urban development intensity gradient in China. Sci. Total Environ. 544, 617–626. https://doi.org/10.1016/j.scitotenv.2015.11.168.
Zhou, D., Xiao, J., Bonafoni, S., Berger, C., Deilami, K., Zhou, Y., Frolking, S., Yao, R., Qiao, Z., Sobrino, J.A., 2019. Satellite remote sensing of surface urban heat islands: progress, challenges, and perspectives. Remote Sens. 11, 48. https://doi.org/10.3390/rs11010048.